

# Towards Understanding the Adversarial Vulnerability of Skeleton-based Action Recognition

Tianhang Zheng<sup>1</sup>, Sheng Liu<sup>2</sup>, Changyou Chen<sup>2</sup>, Junsong Yuan<sup>2</sup>, Baochun Li<sup>1</sup>, Kui Ren<sup>3</sup>

<sup>1</sup>University of Toronto, <sup>2</sup>State University of New York at Buffalo, <sup>3</sup>Zhejiang University

## ABSTRACT

Skeleton-based action recognition has attracted increasing attention due to its potentially broad applications such as autonomous and anonymous surveillance. With the help of deep learning techniques, it has also witnessed substantial progress and achieved excellent accuracy in non-adversarial environments. However, in practice, potential adversaries might easily deceive an action recognition model by performing actions with imperceptible perturbations. Deploying such a model without understanding its adversarial vulnerability might lead to severe consequences, e.g., recognizing a violent action as a normal one. Despite these security concerns, research on the vulnerability of skeleton-based action recognition remains scant, partly due to the challenges caused by the unique nature of human skeletons and actions. Specifically, we argue that for imperceptible and reproducible adversarial skeleton actions: 1) the bone lengths should be maintained roughly the same as the original bone lengths; 2) the changes of joint angles should be small; 3) the adversarial motion speeds should be restricted. These unique constraints hinder direct applications of existing attack methods to adversarial skeleton actions.

In this paper, we conduct a thorough study towards understanding the adversarial vulnerability of skeleton-based action recognition. We first formulate the generation of adversarial skeleton actions as a constrained optimization problem by representing or approximating the constraints with mathematical equations. To deal with the intractable primal optimization problem with equality constraints, we propose to optimize its unconstrained dual problem using ADMM. We further design an efficient plug-in defense, inspired by recent theories and empirical observations, against adversarial skeleton actions. Extensive evaluations demonstrate the effectiveness of our attack and defense, and reveal the properties of adversarial skeleton actions.

## 1 INTRODUCTION

Action recognition is an important task in multimedia and computer vision, motivated by many downstream applications such as video surveillance and indexing, and human-machine interaction [6]. It is also a challenging task since it requires capturing long-term spatial-temporal motion patterns to understand the semantics of actions. Many recent works from the multimedia & computer vision community [10, 16, 30, 31, 35, 42] propose to learn action recognition on the human skeleton motion captured by cameras or depth sensors, where an action is represented by a time series of poses represented as 3D body skeletons. Compared with video streams, skeleton representation is more robust to the variance of background clutters, and also easier-to-handle for machine learning models due to its compact representation. Recent advances in deep learning techniques have been applied to skeleton-based action recognition, including convolutional neural networks [16, 21],



**Figure 1: The targeted setting: misleading the model to recognize “kicking person” as “drinking water” (normal action) by perturbing the skeleton action. To launch the attack in a real-world scenario (e.g., under a surveillance camera), the adversarial skeleton action should satisfy certain constraints. The figure is drawn based on [29].**

recurrent neural networks [22, 32], and graph neural networks [10, 24, 31, 40]. On the other hand, existing work has demonstrated the vulnerability of deep learning techniques to adversarial examples in many application domains, such as face recognition and object detection. This phenomenon motivates us to suspect that, despite achieving high accuracy in non-adversarial environments, the deep neural networks (DNNs) for skeleton-based action recognition might also be vulnerable to adversarial skeleton actions.

It is worth noting that a thorough study on the adversarial vulnerability of action-recognition models is indispensable before deploying them to real-world applications such as surveillance systems. Otherwise, the potential adversaries might easily deceive those systems by performing specific adversarial actions, leading to significant consequences, as shown in Fig. 1. To our knowledge, the study on adversarial skeleton actions is scant and non-trivial<sup>\*</sup>, due to the fundamental differences between the properties of adversarial skeleton actions and other adversarial examples. The differences are caused by the bones between joints and the joint angles, which impose unique spatial constraints on skeleton data [29]. Specifically, in the generated adversarial skeleton actions, lengths of bones must be maintained the same, and simultaneously, joint angles cannot violate certain physiological structures. In addition, considering the physical properties of human bodies, the speeds of motions in the adversarial actions should also be constrained. *If any constraint is not satisfied, the adversarial skeleton actions might be easily perceived and detected or could not be performed by the actors.*

To understand the adversarial vulnerability of skeleton-based action recognition, we first study how to generate adversarial skeleton actions. Specifically, we formulate the generation of adversarial skeleton actions as a constrained optimization problem by representing the spatio-temporal constraints with mathematical equations. Since the primal constrained problem is intractable, we turn

<sup>\*</sup>The only parallel work is detailed in section 2.3.

to solve its dual problem. Moreover, since all the constraints are represented by mathematical equations, both primal and dual variables become unconstrained in the dual problem. We further specify an efficient algorithm based on ADMM to solve the unconstrained dual problem, in which the internal minimization objective is optimized by an Adam optimizer, and the external maximization objective is optimized by one-step gradient ascent. We show that this algorithm can find an adversarial skeleton action within a couple of hundred internal steps.

Other than the attack, we further propose an efficient defense against adversarial skeleton actions based on recent theories and empirical observations. Our defense consists of two core steps, *i.e.*, adding Gaussian noise and Gaussian filtering to action data. The first step, adding Gaussian noise, is inspired by the recent advance in certified defenses. Specifically, adding Gaussian noise to the input is proved to be a certified defense, which means additive Gaussian noise on the adversarial examples can guarantee the model to output a correct prediction (with high probability), as long as the adversarial perturbation is restricted within a certain radius in the neighbor of the original data sample. Note that there are several other methods to certify model robustness, such as dual approach, interval analysis, and abstract interpretations [8, 13, 27, 36, 38]. We adopt the Gaussian noise method because it is simple, effective, and more importantly, scalable to complicated models. Note that skeleton-based action recognition models are always more complicated than the common ConvNets certified by [8, 13, 27, 36, 38]. The second step is to smooth the skeleton frames along the temporal axis using a Gaussian filter. This step will not affect the robustness certified by the first step according to the post-processing property [7, 19, 20], but can always filter out a certain amount of adversarial perturbation and random noise in practice, thus making our defense applicable to normally trained models.

Our proposed attack and defense are evaluated on two open-source models, *i.e.*, 2s-AGCN and HCN [21, 31]<sup>†</sup>. Extensive evaluations show that our attack can achieve 100% attack success rate with almost no violation of the constraints. Moreover, the visualization results, including images and videos, demonstrate that the difference between the original and adversarial skeleton actions is imperceptible. Extensive evaluations also show that our defense is effective and efficient. Specifically, our defense can improve the empirical accuracy of normally trained models to over 60% against adversarial skeleton actions under different settings.

To summarize, our main contribution is three-fold:

- (1) We identify the constraints needed to be considered in adversarial skeleton actions, and formulate the problem of generating adversarial skeleton actions as a constrained optimization problem by formulating those constraints as mathematical equations. We further propose to solve the primal constrained problem by optimizing its dual problem using ADMM, achieving 100% attack success rate.
- (2) We propose an efficient two-step defense against adversarial skeleton actions based on previous theories and empirical observations, and specify the defense in both inference and

<sup>†</sup>We select these two models because the authors have released the code and hyperparameters on Github so that we can correctly reproduce the results. Also, these two models achieve fairly good performance.

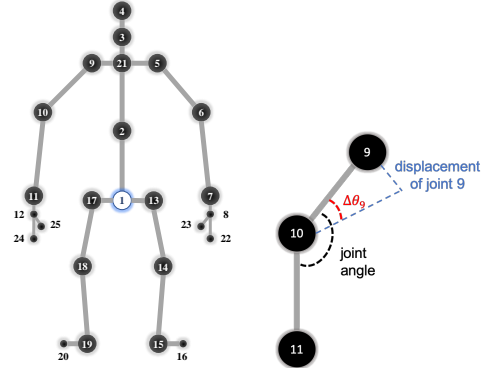


Figure 2: Skeleton Representation

certification stages. The proposed defense achieves high robust accuracy under mild perturbations.

- (3) We conduct extensive evaluations on two open-source models and two datasets. We also provide several interesting observations regarding the properties of adversarial skeleton actions based on the experimental results.

## 2 PRELIMINARIES

### 2.1 Definitions and Notations

Let  $\mathbf{x}$  and  $l \in \{1, 2, \dots, L\}$  respectively denote a data sample and the label, where  $L$  is the number of all possible classes. For an image,  $\mathbf{x}$  is a 2D matrix. For a skeleton action studied in this paper,  $\mathbf{x} \triangleq \{(x_i^\tau, y_i^\tau, z_i^\tau)_{i=1}^I\}_{\tau=1}^{\mathcal{T}}$ , where  $(x_i^\tau, y_i^\tau, z_i^\tau)$  denotes the position (coordinates) of the  $i$ -th joint of the  $\tau$ -th skeleton frame in an action sequence, with  $I$  and  $\mathcal{T}$  denoting the number of joints in a skeleton and the number of skeleton frames in an action sequence, respectively. The corresponding adversarial skeleton action is denoted by  $\mathbf{x}' \triangleq \{(x_i'^\tau, y_i'^\tau, z_i'^\tau)_{i=1}^I\}_{\tau=1}^{\mathcal{T}}$ . We take the skeletons in the largest dataset, *i.e.*, NTU RGB+D dataset, as an example. As shown in Fig. 2, in a skeleton, there are totally 25 joints in a skeleton frame, and thus  $I = 25$ . The number of frames  $\mathcal{T}$  differs for each skeleton action, and usually, we subsample a constant number of frames from each sequence or pad zeros after each sequence to endow all the skeleton actions with the same  $\mathcal{T}$ . Let  $F_\Theta(\cdot)$  denote a classification network, where  $\Theta$  represents the network weights. The logit output on  $\mathbf{x}$  is denoted by  $F_\Theta(\mathbf{x})$  with  $L$  elements  $(\{F_{\Theta,k}(\mathbf{x}) \mid k = 1, \dots, L\})$ .  $F_\Theta(\cdot)$  can correctly classify  $\mathbf{x}$  iff  $\arg\max_k F_{\Theta,k}(\mathbf{x}) = l$ . The goal of adversarial attacks is to find an adversarial sample  $\mathbf{x}'$ , which satisfies several pre-defined constraints, such that  $\arg\max_k F_{\Theta,k}(\mathbf{x}') \neq l$  or  $\arg\max_k F_{\Theta,k}(\mathbf{x}') = l_t$  ( $l_t$  is the target label). A commonly-used constraint is that  $\mathbf{x}'$  should be close to the original sample  $\mathbf{x}$  according to some distance metric.

### 2.2 DNNs for Skeleton-based Action Recognition

In the following, we briefly introduce the two DNNs used for evaluation of our proposed attack method in this project. HCN is a CNN-based end-to-end hierarchical network for learning global co-occurrence features from skeleton data [21]. HCN is designed to learn different levels of features from both raw skeleton and

skeleton motion. The joint-level features are learned by a multi-layer CNN, and the global co-occurrence features are learned from the fused joint-level features. At the end, the co-occurrence features are also fed to a fully-connected network for action classification. 2s-AGCN is one of the state-of-the-art GCN-based models for skeleton-based action recognition. In contrast to the earliest GCN-based model, (*i.e.*, ST-GCN), 2s-AGCN learns the appropriate graph topology of every skeleton action rather than refine the graph topology. This enables 2s-AGCN to capture the implicit connections between joints in certain actions, such as the connection between hand and face in the “wiping face” action. Besides, 2s-AGCN also adopts the two-stream framework to learn from both static and motion information. Overall, 2s-AGCN significantly improves the accuracy of ST-GCN by nearly 7%.

### 2.3 Adversarial Attacks

After the discovery of adversarial examples, the community has developed hundreds of attack methods to generate adversarial samples. In the following, we mainly introduce four attack methods plus a parallel work, with a discussion on the difference between our proposed method and these attacks.

*Fast Gradient Sign Method (FGSM)*. FGSM is a typical one-step adversarial attack algorithm proposed by [11]. The algorithm updates a benign sample along the direction of the gradient of the loss w.r.t. the sample. Formally, FGSM follows the update rule as

$$\mathbf{x}' = \text{clip}_{[v_{min}, v_{max}]} \{ \mathbf{x} + \epsilon \cdot \text{sign}(\nabla_{\mathbf{x}} \mathcal{L}(\Theta, \mathbf{x}, l)) \}, \quad (1)$$

where  $\epsilon$  controls the maximum  $\ell_{\infty}$  perturbation of the adversarial samples;  $[v_{min}, v_{max}]$  is the valid element-wise value range and  $\text{clip}_{[a, b]}(\cdot)$  function clips its input into the range of  $[a, b]$ .

*Projected Gradient Descent (PGD)*. PGD [17, 25] is a strong iterative version of FGSM, which executes Eq. 2.3 for multiple steps with a smaller step size and then projects the updated adversarial examples into the pre-defined  $\ell_p$ -norm ball. Specifically, in each step, PGD updates the sample by

$$\mathbf{x}'_{t+1} = \text{Proj} \{ \mathbf{x}'_t + \alpha \cdot \text{sign}(\nabla_{\mathbf{x}'_t} \mathcal{L}(\Theta, \mathbf{x}'_t, l)) \} \quad (2)$$

The *Proj* function is a clip function for  $\ell_{\infty}$ -norm balls, and an  $\ell_2$  normalizer for  $\ell_{\infty}$ -norm balls.

*Carlini and Wagner Attack*. [5] proposes an attack called C&W attack, which generates  $\ell_p$ -norm adversarial samples by optimization over the C&W loss:

$$\min_{\mathbf{x}'} D(\mathbf{x}, \mathbf{x}') + c \cdot \text{loss}(\mathbf{x}') . \quad (3)$$

In the C&W loss,  $D(\mathbf{x}, \mathbf{x}')$  represents some distance metric between the benign sample  $\mathbf{x}$  and the adversarial sample  $\mathbf{x}'$ , and the metrics used in [5] include  $\ell_{\infty}$ ,  $\ell_0$ , and  $\ell_2$  distances.  $\text{loss}(\cdot)$  is a customized loss. It is worth noting that our proposed attack is completely different from PGD or C&W attack. For PGD, C&W, or many other attacks, the simple constraints on the pixel value can be resolved by projection functions or naturally incorporated into the objective by *sigmoid/tanh* function. However, in our scenario, the constrained optimization problem is much more complicated, and thus has to be solved by more advanced methods.

*ADMM-based Attack*. [44] also proposes a framework based on ADMM to generate  $\ell_p$  adversarial examples. However, we note that our proposed attack is completely different from theirs in two aspects: First, the constraints we consider in this paper are much more complicated than the  $\ell_p$ -norm constraints in [44]. Second, we formulate the problem in a very different manner. Specifically, [44] follows the ADMM framework to break the problem defined like Eq. 3 into two sub-problems; while our attack formulates a different problem with indispensable equality constraints, where ADMM is a natural solution to this problem.

*Adversarial Attack on Skeleton Action*. Note that [23] is a parallel work that proposes an attack based on FGSM and BIM (PGD) to generate adversarial skeleton actions. Specifically, [23] adapts the FGSM and BIM to skeleton-based action recognition by using a clipping function and an alignment operation to impose the bone and joint constraints on the updated adversarial skeleton actions in each iteration. *However, [23] is very different from our work*. First, the joint constraints considered in [23] are not the constraints for joint angles mentioned before. Second, the alignment operation might corrupt the perturbation learned in each iteration. In contrast to [23], we attempt to formulate adversarial skeleton action generation as a constrained optimization problem with equality constraints. Releasing the equality constraints by Lagrangian multipliers yields an unconstrained dual optimization problem, which does not need any complicated additional operation in the optimization process. Third, we propose to solve the the dual optimization problem by ADMM, which is a more appropriate method to optimize complicated constrained problems. Therefore, the attack achieves better performance than [23], which will be detailed in section 6.1. Finally, we specify a defense method against adversarial skeleton actions based on the state-of-the-art theories and our observations.

### 2.4 Alternating Direction Method of Multipliers (ADMM)

Alternating Direction Method of Multipliers (ADMM) is a powerful optimization algorithm to handle large-scale statistical tasks in diverse application domains. It blends the decomposability of dual ascent with the great convergence property of the method of multipliers. Currently, ADMM plays a significant role in solving statistical problems, such as support vector machines [9], trace norm regularized least squares minimization [41], and constrained sparse regression [3]. Except for convex problems, ADMM is also a widely used solution to some nonconvex problems, whose objective function could be nonconvex, nonsmooth, or both. [37] shows that ADMM is able to converge as long as the objective has a smooth part, while the remaining part can be coupled or nonconvex, or include separable nonsmooth functions. Applications of ADMM to nonconvex problems include network reference [26], global conformal mapping [18], noisy color image restoration [18].

### 2.5 Adversarial Defenses

Both learning and security communities have developed many defensive methods against adversarial examples. Among them, adversarial training and several certified defenses attract the most attention due to their outstanding/guaranteed performance against strong attacks [2, 14, 34]. In the following, we briefly introduce

adversarial training and several certified defenses, including the randomized smoothing method adopted in this paper.

*Adversarial Training.* Adversarial training is one of the most successful empirical defenses in the past few years [11, 25, 43]. The intuition of adversarial training is to improve model robustness by training the model with adversarial examples. Although adversarial training achieves tremendous success against many strong attacks [1, 33, 45], its performance is not theoretically guaranteed and thus might be compromised in the future. Besides, adversarial training always requires much more computational resource than standard training, making it not scalable to complicated models.

*Certified Defenses.* A defense with a theoretical guarantee on its defensive performance is considered as a certified defense. In general, there are three main approaches to design certified defenses. The first approach is to formulate the certification problem as an optimization problem and bound it by dual approach and convex relaxations [8, 28, 38]. The second approach approximates a convex set that contains all the possible outputs of each layer to certify an upper bound on the range of the final output [13, 27, 36]. The third is the randomized smoothing method used in this paper. The only essential operation for this method is to add Gaussian/Laplace noise to the inputs, which is simple and applicable to any deep learning models. [19] first proves that randomized smoothing is a certified defense by theories on differential privacy. [20] improves the certified bound using a lemma on Renyi divergence. Cohen et al. [7] proves a tight bound on the  $\ell_2$  robust radius certified by adding Gaussian noise using the Neyman-Pearson lemma. [15] further extends the approach of [7] to the *top-k* classification setting. Since the bound proved by [7] is the tightest, the method in [7] is used for certification. In this paper we adopt the approach in [19] due to its ability for efficient inference in practice.

### 3 THREAT MODEL

#### 3.1 Adversary Knowledge: White-box Setting

In this paper, we follow the white-box setting, where the adversary has full access to the model architecture and parameters. We make this assumption because (i) it is always a safe, conservative, and realistic assumption since we might never know the knowledge of potential adversaries about the model [5], which varies among different adversaries and also changes over time. (ii) For systems/devices equipped with an action recognition model, recognition is more likely to be done locally, or on a local cloud, making the adversary easily acquire the model parameters with his own system/device. Note that although most of the experiments on the proposed attack and defense are done under the white-box setting, we also have several experiments on evaluating the transferability of our attack.

#### 3.2 Adversary Goal: Targeted & Untargeted label Setting

Under the targeted setting, the goal of an adversary is to mislead the recognition model to predict the adversarial skeleton action as a targeted label pre-defined by the adversary. For instance, suppose the adversary is “kicking” someone under a surveillance camera

equipped with an action recognition model. It may launch a targeted attack to mislead the model to recognize this violent action as a normal one such as “drinking water”. Under the untargeted label settings, an adversary only aims to disable the recognition and thus is considered successful as long as the model makes wrong predictions instead of a specific targeted prediction. In this paper, we propose two objectives suitable for the above two settings respectively, which will be detailed in section 4.4.

#### 3.3 Imperceptibility & Reproducibility

Except for the aforementioned adversary goals, the adversary also requires the adversarial perturbation to be both imperceptible and reproducible. Here “imperceptibility” means it should be difficult for human vision to figure out the difference between the original and adversarial skeleton actions. Imperceptibility is not only a common requirement in the previous attacks, but also a useful one in our scenario. Note that it is natural to schedule a periodical examination for an autonomous surveillance system by human labor to check if the system works well. If the system has been fooled by a seemingly “normal” adversarial skeleton action, the mistake might be considered due to the system itself rather than the adversary who performs the adversarial skeleton action in the examination process. Here “reproducibility” is an additional requirement specific to our scenario. As mentioned in the introduction, the adversarial skeleton action could be a real threat when it can be reproduced under a real-world system. Thus, to make our attack a real-world threat, the generated adversarial skeleton actions should satisfy three concrete constraints to be imperceptible and reproducible, which will be detailed in section 4.

### 4 ADVERSARIAL SKELETON ACTION

In this section, we present our proposed attack, *i.e.*, ADMM attack. We first introduce how to formulate the three constraints into mathematical equations. Then we formulate the constrained optimization problem to generate adversarial skeleton actions under both targeted and untargeted settings. Finally, we elaborate on how to solve the optimization problem by ADMM.

#### 4.1 Bone Constraints

We again take the skeletons in the NTU RGB+D dataset as an example. As shown in Fig. 2, in a skeleton, there are totally 25 joints, forming a total of 24 bones. While the bones are not explicitly considered in modeling, they are strictly connecting to the 25 joints, thus imposing 24 bone-length constraints, *i.e.*, the distance between the joints at the two ends of a bone should remain the same in adversarial skeleton actions. To mathematically represent the 24 bones, we associate each joint with its preceding joint, forming the two ends of a bone. As a result, the 24 preceding-joints for joint-2~joint-25 are denoted as  $\mathcal{P} \triangleq \{(x_{pi}^r, y_{pi}^r, z_{pi}^r)_{i=2}^{25}\}$ . The corresponding joint indices of the elements in  $\mathcal{P}$  are {1, 21, 3, 21, 5, 6, 7, 21, 9, 10, 11, 1, 13, 14, 15, 1, 17, 18, 19, 2, 8, 8, 12, 12}. We define the *i*-th bone’s length as  $B_i^r \triangleq \sqrt{(x_i^r - x_{pi}^r)^2 + (y_i^r - y_{pi}^r)^2 + (z_i^r - z_{pi}^r)^2}$ . In this regard, the bone constraints can be represented as  $B_i^r = B_i^{r'}$ . Due to the measurement errors in the NTU dataset itself, here we also tolerate very small difference between  $B_i^r$  and  $B_i^{r'}$ . Therefore,

we can finally formulate the bone constraints as

$$|B_i^{\tau} - B_i^{\tau}|/B_i^{\tau} \leq \epsilon_L, \quad (4)$$

where  $\epsilon_L$  is usually set as 0.01  $\sim$  0.03. *Note that inequality constraints in the primal problem will impose inequality constraints on the corresponding Lagrangian variables in the dual problem.* In order to avoid this in the dual problem, we reformulate the above inequality constraints as mathematical equations, i.e., (4) is equivalent to

$$\max\{|B_i^{\tau} - B_i^{\tau}|/B_i^{\tau} - \epsilon_L, 0\} = 0. \quad (5)$$

## 4.2 Joint Angle Constraints

Except for the bone-length constraints, we also need to impose constraints on the rotations of the joint angles according to the physiological structures of human beings. Let us also use the NTU dataset as an example. Each joint angle corresponds to the angle between two bones, and thus can be represented by the three joint locations of those two corresponding bones as illustrated in the right of Fig. 2. Note that a natural way to compute the joint angle as shown in Fig. 2 is to first compute the cosine value and then input the value into the arccos function. However, the gradient of arccos function is likely exploded, causing large numerical errors when the cos value of the joint angle is close to 1 ( $\frac{d}{dx} \arccos x = -\frac{1}{\sqrt{1-x^2}}$ ). To deal with this issue, we derive an approximate upper bound for the changes of joint angle value to avoid computing the arccos function and its gradient. Again, take the right of Fig. 2 as an example, the angle change  $\Delta\theta_9$  caused by the displacement of joint-9 (i.e.,  $x_9^{\tau} - x_9^{\tau}, y_9^{\tau} - y_9^{\tau}, z_9^{\tau} - z_9^{\tau}$ ) can be approximated

by  $\sin \Delta\theta_9 \approx \frac{\sqrt{(x_9^{\tau} - x_9^{\tau})^2 + (y_9^{\tau} - y_9^{\tau})^2 + (z_9^{\tau} - z_9^{\tau})^2}}{\sqrt{(x_{10}^{\tau} - x_9^{\tau})^2 + (y_{10}^{\tau} - y_9^{\tau})^2 + (z_{10}^{\tau} - z_9^{\tau})^2}}$ . In particular, when

the angle change  $\Delta\theta$  is smaller than 0.1 (i.e.,  $5.73^\circ$ ), we can consider  $\sin \Delta\theta$  almost same as  $\Delta\theta$ . The total angle change  $\Delta\theta$  is upper bounded by the sum of the changes caused by the displacements of joint-9, joint-10, and joint-11. Therefore the upper bound can be represented by  $J^{\tau} =$

$$\frac{\sqrt{(x_9^{\tau} - x_9^{\tau})^2 + (y_9^{\tau} - y_9^{\tau})^2 + (z_9^{\tau} - z_9^{\tau})^2}}{\sqrt{(x_{10}^{\tau} - x_9^{\tau})^2 + (y_{10}^{\tau} - y_9^{\tau})^2 + (z_{10}^{\tau} - z_9^{\tau})^2}} + \frac{\sqrt{(x_{10}^{\tau} - x_{10}^{\tau})^2 + (y_{10}^{\tau} - y_{10}^{\tau})^2 + (z_{10}^{\tau} - z_{10}^{\tau})^2}}{\sqrt{(x_{11}^{\tau} - x_{10}^{\tau})^2 + (y_{11}^{\tau} - y_{10}^{\tau})^2 + (z_{11}^{\tau} - z_{10}^{\tau})^2}} + \frac{\sqrt{(x_{11}^{\tau} - x_{11}^{\tau})^2 + (y_{11}^{\tau} - y_{11}^{\tau})^2 + (z_{11}^{\tau} - z_{11}^{\tau})^2}}{\sqrt{(x_{11}^{\tau} - x_{10}^{\tau})^2 + (y_{11}^{\tau} - y_{10}^{\tau})^2 + (z_{11}^{\tau} - z_{10}^{\tau})^2}}$$

Although this representation looks more complicated than the arccos function, its gradient can be computed efficiently and accurately. Given such an approximation, the joint angle constraints can be similarly represented as

$$\max\{J_k^{\tau} - \epsilon_J, 0\} = 0 \quad (6)$$

where  $\epsilon_J$  is set as 0.1  $\sim$  0.2 ( $6^\circ \sim 12^\circ$ ). *Note that  $J_k^{\tau}$  represents the approximation of the change of a joint angle.*

## 4.3 Speed Constraints

According to the physical conditions of human beings, we should consider one more type of constraints, i.e., temporal smoothness constraints. By those constraints, we attempt to restrict the speeds of the motions in the generated adversarial skeleton actions. Specifically, the speeds of the motions can be approximated by the displacements between two consecutive temporal frames, i.e.,  $S_m^{\tau} \approx \sqrt{(x_m^{\tau+1} - x_m^{\tau})^2 + (y_m^{\tau+1} - y_m^{\tau})^2 + (z_m^{\tau+1} - z_m^{\tau})^2}$ . Then, similar to Eq. 5,

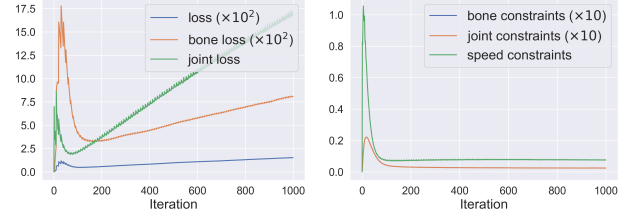


**Figure 3: Evolution of the averaged loss items and the constraints ( $\beta = 1.0$ )**

we bound the change of speeds by

$$\max\{|S_m^{\tau} - S_m^{\tau}|/S_m^{\tau} - \epsilon_S, 0\} = 0, \quad (7)$$

where  $\epsilon_S$  is usually set as (smaller than) 10%.

## 4.4 Constrained Primal Problem Formulation

In this subsection, we introduce the main objectives used under the untargeted setting and targeted setting.

*Untargeted Setting.* Under the untargeted setting, the adversary achieves its goal as long as the DNN makes a prediction other than the ground-truth label, i.e.,  $\text{argmax}_k F_{\Theta, k}(\mathbf{x}') \neq l$ . This will hold iff  $F_{\Theta, l}(\mathbf{x}') < \max_{k, k \neq l} F_{\Theta, k}(\mathbf{x}')$ . Therefore, we define the objective as minimizing  $\max\{F_{\Theta, l}(\mathbf{x}') - \max_{k, k \neq l} F_{\Theta, k}(\mathbf{x}') + \text{conf}, 0\}$ , where  $\text{conf} > 0$  is the desired confidence value of the DNN on the wrong prediction. Note that if the objective is equal to 0, we have  $\max_{k, k \neq l} F_{\Theta, k}(\mathbf{x}') \geq F_{\Theta, l}(\mathbf{x}') + \text{conf}$ .

*Targeted Setting.* The goal of the adversary is to render the prediction result to be the attack target  $l_t$ , i.e.,  $\text{argmax}_{k \in \mathcal{K}} F_{\Theta, k}(\mathbf{x}') = l_t$ . Therefore, the primal objective is defined as minimizing the cross entropy between  $F_{\Theta, k}(\mathbf{x}')$  and  $l_t$ , or  $\max\{\max_{k, k \neq l_t} F_{\Theta, k}(\mathbf{x}') - F_{\Theta, l_t}(\mathbf{x}') + \text{conf}, 0\}$  following the logic of the untargeted setting.

We can also adopt other objectives for our purpose. However, it turns out the above two main objectives are the most commonly-used ones in previous work [5, 17, 25]. For simplicity, we denote the main loss by  $\mathcal{L}(\mathbf{x}, l)$ . The constrained primal problem can be formulated as

$$\min_{\mathbf{x}'} \mathcal{L}(\mathbf{x}', l) \quad (8)$$

subject to Eq. (5), (6), (7)

## 4.5 Dual Optimization by ADMM

Note that our constrained primal problems are in general intractable. Instead of searching for a solution to the constrained primal problem, we propose to formulate and optimize its unconstrained dual problem via ADMM. The algorithm is illustrated in Alg. 1. Specifically, we first define the augmented Lagrangian of the constrained primal as shown in Alg. 1. The additional term  $\frac{\beta}{2} (\|B'\|_2^2 + \|J'\|_2^2 + \|S'\|_2^2)$ , which is commonly used in ADMM (for nonconvex problems), aims to further penalize any violation of the equality constraints. *We note that larger  $\beta$  usually leads to smaller violation but larger final main objective (decreases the attack success rate).*

Specifically, given the Lagrangian  $\mathcal{G}(\mathbf{x}, l; \lambda, \nu, \omega)$  (defined in Alg. 1), the dual problem is  $\max_{\lambda, \nu, \omega} \min_{\mathbf{x}'} \mathcal{G}(\mathbf{x}, l; \lambda, \nu, \omega)$ . Note that



since the internal function  $\min_{\mathbf{x}'} \mathcal{G}(\mathbf{x}, l; \boldsymbol{\lambda}, \boldsymbol{\nu}, \boldsymbol{\omega})$  is an affine function w.r.t. the variables  $\boldsymbol{\lambda}, \boldsymbol{\nu}, \boldsymbol{\omega}$ , we can simply use single-step gradient ascent with a large step size (usually set as  $\beta$  in ADMM) to update those dual variables. However,  $\mathcal{G}(\mathbf{x}, l; \boldsymbol{\lambda}, \boldsymbol{\nu}, \boldsymbol{\omega})$  is an extremely complicated nonconvex function w.r.t. the adversarial sample  $\mathbf{x}'$ . Therefore, in most cases, we could only guarantee local optima for the internal minimization problem. Fortunately, it turns out that even the local optima can always fool the DNNs. To find a local optimum efficiently, we adopt the Adam optimizer instead of the vanilla stochastic gradient descent (SGD) since Adam optimizer always converges faster than vanilla SGD. Theoretically, a local minimum is guaranteed because the Adam optimizer stops updating the variables when the gradients are (close to) 0. Next, we further look into the evolution of the loss during the optimization process. As shown in Fig. 3, at the very beginning (*i.e.*, the first stage), the internal minimization problem finds adversarial samples with large violation of the constraints. The large violation will cause the Lagrangian multipliers  $\boldsymbol{\lambda}, \boldsymbol{\nu}, \boldsymbol{\omega}$  to increase rapidly, and thus significantly increase the loss terms  $\langle \boldsymbol{\lambda}, \mathbf{B}' \rangle$  (bone loss),  $\langle \boldsymbol{\nu}, \mathbf{J}' \rangle$  (joint loss), and  $\langle \boldsymbol{\omega}, \mathbf{S}' \rangle$  (speed loss). As a result, the algorithm proceeds into the second stage, where the Adam optimizer focuses more on diminishing the constraint violation  $\mathbf{B}', \mathbf{J}'$ , and  $\mathbf{S}'$  when optimizing  $\mathbf{x}'$ . Finally, the algorithm proceeds into a relatively stable stage where we can stop the algorithm. According to Fig. 2, our algorithm is very efficient in the sense that it only needs 200 (internal) iterations to enter the final stable stage.

---

#### Algorithm 1 Generating Adversarial Skeleton Actions

---

**Require:** Loss function  $\mathcal{L}(\mathbf{x}, l)$ , hyper-parameter  $\beta$ , adam optimizer for the adversarial skeleton action  $\mathbf{x}'$ , maximum number of iterations  $T$ .

**Define Constraints:**  $B_j^{\prime\tau} \triangleq \max\{|B_j^{\prime\tau} - B_j^\tau|/B_j^\tau - \epsilon_L, 0\}$ ,  $J_k^{\prime\tau} \triangleq \max\{J_k^{\prime\tau} - \epsilon_J, 0\}$ , and  $S_m^{\prime\tau} \triangleq \max\{|S_m^{\prime\tau} - S_m^\tau|/S_m^\tau - \epsilon_S, 0\}$ . (Vector Representations:  $\mathbf{B}', \mathbf{J}'$ , and  $\mathbf{S}'$ )

**Define Lagrangian Variables:**  $\boldsymbol{\lambda}, \boldsymbol{\nu}$ , and  $\boldsymbol{\omega}$  (Corresponding to  $\mathbf{B}', \mathbf{J}'$ , and  $\mathbf{S}'$ )

**Define Augmented Lagrangian:**  $\mathcal{G}(\mathbf{x}, l; \boldsymbol{\lambda}, \boldsymbol{\nu}, \boldsymbol{\omega}) \triangleq \mathcal{L}(\mathbf{x}, l) + \langle \boldsymbol{\lambda}, \mathbf{B}' \rangle + \langle \boldsymbol{\nu}, \mathbf{J}' \rangle + \langle \boldsymbol{\omega}, \mathbf{S}' \rangle + \frac{\beta}{2} (\|\mathbf{B}'\|_2^2 + \|\mathbf{J}'\|_2^2 + \|\mathbf{S}'\|_2^2)$ .

**for**  $t = 0$  to  $T - 1$  **do**

**Update**  $\mathbf{x}'$ : fix the multipliers  $\boldsymbol{\lambda}(t), \boldsymbol{\nu}(t), \boldsymbol{\omega}(t)$

$\mathbf{x}'(t + 1) \in \operatorname{argmin}_{\mathbf{x}'} \mathcal{G}(\mathbf{x}', l; \boldsymbol{\lambda}(t), \boldsymbol{\nu}(t), \boldsymbol{\omega}(t))$  updated by the adam optimizer

**Update Multipliers:** compute  $\mathbf{B}'(t + 1), \mathbf{J}'(t + 1)$ , and  $\mathbf{S}'(t + 1)$  based on  $\mathbf{x}'(t + 1)$

$\boldsymbol{\lambda}(t + 1) = \boldsymbol{\lambda}(t) + \beta \mathbf{B}'(t + 1)$ ;  $\boldsymbol{\nu}(t + 1) = \boldsymbol{\nu}(t) + \beta \mathbf{J}'(t + 1)$ ;

$\boldsymbol{\omega}(t + 1) = \boldsymbol{\omega}(t) + \beta \mathbf{S}'(t + 1)$

**end for**

**Output**  $\mathbf{x}'(T)$

---

## 5 DEFENSE AGAINST ADVERSARIAL SKELETON ACTIONS

Note that although the method proposed in [7, 20] can certify larger robust radii than [19]. However, the sample complexity to compute

the confidence intervals in [7, 20] will lead to computational overhead in the inference stage. *Therefore, we only use the method in [7] in the certification process. In the inference stage, we modify the method in [19] to build a relatively efficient defense against adversarial skeleton actions, as shown in Alg. 2.* In general, our proposed defense consists of two steps: adding Gaussian noise and temporal filtering by Gaussian kernel. In the following, we will detail these two steps and explain why we include them in the defense.

### 5.1 Additive Gaussian Noise

Our first step is adding Gaussian noise to the skeleton actions. In the inference stage, we follow [19] to make the prediction as  $\operatorname{argmax}_k E(\mathbf{F}_{\Theta, k}(\mathcal{M}(\mathbf{x}')))$  given input  $\mathbf{x}'$ , where  $\mathcal{M}(\mathbf{x}) = \mathbf{G}(\mathbf{x} + \mathbf{z})$  is randomized mechanism with Gaussian noise  $\mathbf{z}$  and post-processing function  $\mathbf{G}$ . In order to estimate  $E(\mathbf{F}_{\Theta}(\mathcal{M}(\mathbf{x}')))$ , we sample  $N$  noisy samples  $\tilde{\mathbf{x}}'(n) = \mathbf{x}' + \tilde{\mathbf{z}}(n)$  from  $\mathcal{N}(\mathbf{x}', \sigma^2 \mathbf{I})$  and feed them into the post-processing function  $\mathbf{G}$  and the neural network  $\mathbf{F}_{\Theta}$ .  $E(\mathbf{F}_{\Theta}(\mathcal{M}(\mathbf{x}')))$  is estimated by  $\frac{1}{N} \sum_{n=1}^N \mathbf{F}_{\Theta}(\mathbf{G}(\tilde{\mathbf{x}}'(n)))$ , and according to the Chernoff bound [4], the error of this estimation is bounded by

$$\Pr\left(\left|\frac{1}{N} \sum_{n=1}^N \mathbf{F}_{\Theta, l}(\mathbf{G}(\tilde{\mathbf{x}}'(n))) - E(\mathbf{F}_{\Theta, l}(\mathcal{M}(\mathbf{x}')))\right| < \epsilon\right) \sim \mathcal{O}(e^{-N\epsilon^2})$$

In the certification stage, we rely on the main theorem from [7], which gives the currently tightest bound:

LEMMA 1. *Denote an mechanism randomized by Gaussian noise by  $\mathcal{M}(\mathbf{x}) = \mathbf{G}(\mathbf{x} + \mathbf{z})$ , and the ground-truth label by  $l$ . Define  $f(\mathbf{x}) = \operatorname{argmax}_k \mathbf{F}_{\Theta, k}(\mathcal{M}(\mathbf{x}))$ . Suppose  $\underline{p}_A$  &  $\overline{p}_B$  satisfy*

$$\Pr(f(\mathbf{x}) = l) \geq \underline{p}_A \geq \overline{p}_B \geq \max_{i \neq l} \Pr(f(\mathbf{x}) = i), \quad (9)$$

the  $\ell_2$  robust radius is  $R = \frac{\sigma}{2} (\Phi^{-1}(\underline{p}_A) - \Phi^{-1}(\overline{p}_B))$ .

Lemma 1 indicates that as long as  $\|\mathbf{x}' - \mathbf{x}\|_2 < R$ ,  $\operatorname{argmax}_i \Pr(f(\mathbf{x}) = i) = l$ , *i.e.*, the prediction is correct. The algorithm using the above lemma for certification is detailed in Algorithm 3. In the next subsection, we will detail the post-processing function mentioned before.

---

#### Algorithm 2 Defense (Inference)

---

**Require:** Neural Network  $\mathbf{F}_{\Theta}(\cdot)$ , standard deviation of the additive Gaussian noise  $\sigma$ , skeleton action  $\mathbf{x}'$  (probably adversarial), number of noisy samples for inference of  $n$ .

Sample  $N$  samples from  $\mathcal{N}(\mathbf{x}', \sigma^2 \mathbf{I}) \rightarrow \{\tilde{\mathbf{x}}'(n) | n = 1, 2, \dots, N\}$

Smooth  $\tilde{\mathbf{x}}'(n)$  by a  $1 \times 5$  or  $1 \times 7$  Gaussian filter  $\rightarrow \mathbf{G}(\tilde{\mathbf{x}}'(n))$

Feed  $\mathbf{G}(\tilde{\mathbf{x}}'(n))$  into the network  $\rightarrow \mathbf{F}_{\Theta}(\mathbf{G}(\tilde{\mathbf{x}}'(n)))$

**Output**  $\operatorname{argmax}_l \sum_{n=1}^N \mathbf{F}_{\Theta, l}(\mathbf{G}(\tilde{\mathbf{x}}'(n)))$

---

### 5.2 Temporal Filtering by Gaussian Kernel

After adding Gaussian noise to the skeleton actions, we propose to further smooths the action along the temporal axis by a  $1 \times 5$  or  $1 \times 7$  Gaussian filter. The intuition is that the adjacent frames in a skeleton action sequence are very similar to each other, and thus can be used as references to rectify the adversarial perturbations. Although this additional operation does not improve the certification results, we

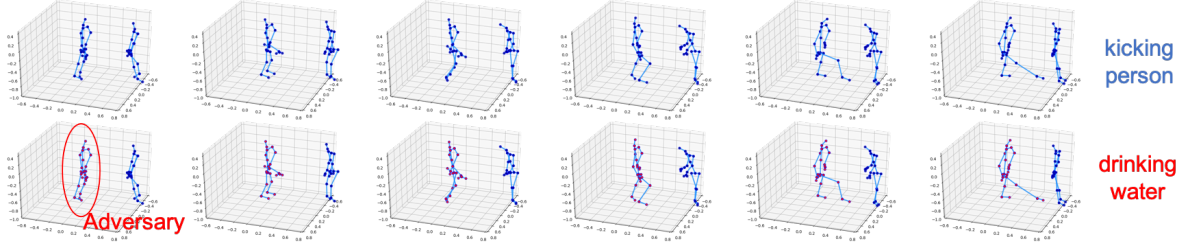


**Figure 4:** The top six frames represent a “kicking (another person)” skeleton action, and the bottom six frames are the corresponding frames from the adversarial skeleton action generated by our attack under the targeted setting (optimizing the first person). The generated adversarial skeleton action is recognized as “drinking water” by the 2s-AGCN.

---

### Algorithm 3 Defense (Certification)

---

**Require:** Neural Network  $F_{\Theta}(\cdot)$ , standard deviation of the additive Gaussian noise  $\sigma$ , original and adversarial skeleton action  $\mathbf{x}$  &  $\mathbf{x}'$ , number of noisy samples for inference of  $n$ , a predefined confidence value  $p$  for hypothesis test (usually 95%).

**Recognition:** Sample  $N$  samples from  $\mathcal{N}(\mathbf{x}, \sigma^2 \mathbf{I}) \rightarrow \{\tilde{\mathbf{x}}(n) | n = 1, 2, \dots, N\}$

Smooth  $\tilde{\mathbf{x}}(n)$  by a  $1 \times 5$  or  $1 \times 7$  Gaussian filter  $\rightarrow \mathbf{G}(\tilde{\mathbf{x}}(n))$

Feed  $\tilde{\mathbf{x}}(n)$  into the (normally trained) network  $\rightarrow F_{\Theta}(\mathbf{G}(\tilde{\mathbf{x}}(n)))$

**Confidence Interval:** Compute the number (counts) top two indices in  $\{\arg\max_k F_{\Theta,k}(\mathbf{G}(\tilde{\mathbf{x}}(n))) | n = 1, 2, \dots, N\} \rightarrow c_A, c_B$   
 Compute the lower bound for  $p_A$  and the upper bound for  $p_B$  by the method in [12] with confidence  $p \rightarrow \underline{p}_A, \overline{p}_B$ .

**Certification:** Compute the certified  $\ell_2$  radius by  $R = \frac{\sigma}{2} (\Phi^{-1}(\underline{p}_A) - \Phi^{-1}(\overline{p}_B))$ .

Output  $\max\{R, 0\}$  if  $p_A$  corresponds to the ground-truth label  $l$   
 else  $-1$  (certified robust radius)

Compare  $R$  with  $\|\mathbf{x}' - \mathbf{x}\|_2$ , and if  $R$  is larger, then output the index corresponding to  $c_A$  (if inputs have  $\mathbf{x}'$ )

---

observe that it can help our defense become more compatible with a normally trained model than the original randomized smoothing method in [7, 19]. Also, we argue that this simple operation is not usually used in previous work because it is not very suitable in the image recognition domain, where no adjacency information (along the temporal axis) is available.

## 6 EXPERIMENTS

### 6.1 Attack Performance

*Main Results.* The main results of our attack are shown in Table 5. As we can see, our proposed attack can achieve 100% success rates with very small violation of the constraints. The averaged normalized bone-length difference is approximately 1% ~ 2%, and the violation of the joint angles is smaller than  $10^\circ$ . *Considering the skeleton data is usually noisy, this subtle violation is considered “very common” in real world.*

We also note that adversarial-sample generation under the untargeted setting is usually easier than that under the targeted setting

since a targeted adversarial sample is guaranteed to be an untargeted adversarial sample, but not vice versa. This fact is also reflected by the results in Table 5. Furthermore, in Fig. 4, we show the visualization result of an adversarial skeleton action (recognized as a normal action “drinking water”) generated by our attack, which is almost visually indistinguishable from its original skeleton action (“kicking”).

*Transferability.* In order to shed light on the transferability of our attack, we feed the adversarial skeleton actions generated on a HCN model to another HCN model and 2s-AGCN, respectively. In order to boost the transferability performance, we set  $\beta$  as 0.01 or 0.1 to generate adversarial skeleton actions with larger perturbation. The attack success rates are given in Table 2. *Similar to 3D adversarial point clouds [39], the transferability of the adversarial skeleton actions is also a little limited compared with adversarial images.*

*Comparison with C&W Attack.* We use C&W attack as an example to shed light on the difference between our attack and the existing attacks. C&W attack has been demonstrated as a successful optimization-based adversarial attack in many application domains. However, since C&W attack mainly considers minimizing the  $\ell_2$  distance between original and adversarial skeletons, it might easily violate the constraints, as shown in our simple case study (Table 3).

### 6.2 Defense Performance

*Empirical Results.* We demonstrate the performance of the defense for inference in Table 4. We set  $\beta = 1.0$  to generate adversarial examples, and set  $N = 50$  (Alg. 2), which is more smaller than the number of samples required for certification but can achieve good empirical performance, as shown in Table 4. *it is much easier to defend adversarial skeleton actions under the targeted setting than the untargeted setting.* Note that the accuracy of HCN on NTU-CV and NTU-CS is respectively 91.1% and 86.5% [21], and the accuracy of 2s-AGCN is respectively 95.1% and 88.5% [31].

*Certified Results.* Due to the high computational cost of the certification method ( $N=1000$ ), we mainly evaluate the certification algorithm on HCN. The certified accuracy achieved by different levels of noise is shown in Fig. 5. Note that we use the same level of noise to train the model as for certification. *As we can see, with sacrificing 10% ~ 20% accuracy on the clean samples, the method is able to achieve about 50% certified accuracy ( $\ell_2 = 0.5$ ).*

| White-box<br>Untargeted | $\beta$ | NTU CV       |              |            |              |          | NTU CS       |              |            |              |          |
|-------------------------|---------|--------------|--------------|------------|--------------|----------|--------------|--------------|------------|--------------|----------|
|                         |         | Success Rate | $\Delta B/B$ | $\Delta J$ | $\Delta K/K$ | $\ell_2$ | Success Rate | $\Delta L/L$ | $\Delta J$ | $\Delta K/K$ | $\ell_2$ |
| HCN                     | 0.1     | 100%         | 2.64%        | 0.132      | 4.52%        | 0.396    | 100%         | 2.17%        | 0.111      | 3.17%        | 0.347    |
|                         | 1.0     | 100%         | 1.92%        | 0.099      | 1.65%        | 0.330    | 100%         | 1.62%        | 0.086      | 1.30%        | 0.290    |
|                         | 10.0    | 92.8%        | 1.50%        | 0.085      | 1.25%        | 0.270    | 92.4%        | 1.25%        | 0.073      | 0.98%        | 0.241    |
| 2s-AGCN                 | 0.1     | 100%         | 2.17%        | 0.112      | 1.62%        | 0.653    | 100%         | 1.97%        | 0.107      | 2.20%        | 0.614    |
|                         | 1.0     | 100%         | 1.70%        | 0.094      | 0.59%        | 0.528    | 100%         | 1.46%        | 0.086      | 0.57%        | 0.496    |
|                         | 10.0    | 99.0%        | 1.37%        | 0.083      | 0.39%        | 0.428    | 98.8%        | 1.19%        | 0.078      | 0.34%        | 0.413    |
| White-box<br>targeted   | $\beta$ | NTU CV       |              |            |              |          | NTU CS       |              |            |              |          |
|                         |         | Success Rate | $\Delta B/B$ | $\Delta J$ | $\Delta K/K$ | $\ell_2$ | Success Rate | $\Delta L/L$ | $\Delta J$ | $\Delta K/K$ | $\ell_2$ |
| HCN                     | 0.1     | 100%         | 3.60%        | 0.165      | 7.75%        | 0.673    | 100%         | 3.55%        | 0.165      | 6.68%        | 0.723    |
|                         | 1.0     | 99.7%        | 3.24%        | 0.156      | 4.69%        | 0.630    | 100%         | 3.16%        | 0.155      | 4.24%        | 0.674    |
|                         | 10.0    | 22.3%        | 2.27%        | 0.115      | 2.83%        | 0.444    | 26.9%        | 2.14%        | 0.112      | 2.50%        | 0.462    |
| 2s-AGCN                 | 0.1     | 100%         | 1.66%        | 0.090      | 0.55%        | 0.569    | 100%         | 1.67%        | 0.091      | 0.71%        | 0.649    |
|                         | 1.0     | 100%         | 1.61%        | 0.091      | 0.42%        | 0.556    | 100%         | 1.56%        | 0.090      | 0.49%        | 0.615    |
|                         | 10.0    | 97.2%        | 1.54%        | 0.089      | 0.38%        | 0.512    | 97.9%        | 1.47%        | 0.087      | 0.40%        | 0.552    |

Table 1: The *empirical* performance of our proposed method: averaged bone-length difference between original and adversarial skeletons ( $\Delta L/L$ ), averaged joint angle difference (upper bound) ( $\Delta J$ ), kinetic energy difference ( $\Delta K/K$ ),  $\ell_2$  distance ( $\ell_2$ ).

| Source (Model) $\rightarrow$ Target | Dataset | $\beta = 0.1$ | $\beta = 0.01$ |
|-------------------------------------|---------|---------------|----------------|
| HCN(1) $\rightarrow$ HCN(2)         | NTU CV  | 24.7%         | 26.0%          |
|                                     | NTU CS  | 28.5%         | 32.6%          |
| HCN(1) $\rightarrow$ 2s-AGCN        | NTU CV  | 16.2%         | 20.4%          |
|                                     | NTU CS  | 17.6%         | 21.8%          |

Table 2: Attack success rates of adversarial examples transferred between models.

| Untargeted | Success Rate | $\Delta B/B$ | $\Delta J$ | $\Delta K/K$ | $\ell_2$ |
|------------|--------------|--------------|------------|--------------|----------|
| NTU CV     | 100%         | 4.67%        | 0.241      | 13.0%        | 0.278    |
| NTU CS     | 100%         | 4.09%        | 0.211      | 10.2%        | 0.244    |
| Targeted   | Success Rate | $\Delta B/B$ | $\Delta J$ | $\Delta K/K$ | $\ell_2$ |
| NTU CV     | 100%         | 8.82%        | 0.468      | 38.1%        | 0.510    |
| NTU CS     | 100%         | 9.45%        | 0.507      | 36.8%        | 0.520    |

Table 3: Adversarial skeleton actions generated by C&W attack on HCN.

| Model   | Setting    | NTU CV          |                 | NTU CS          |                 |
|---------|------------|-----------------|-----------------|-----------------|-----------------|
|         |            | $\sigma = 0.01$ | $\sigma = 0.02$ | $\sigma = 0.01$ | $\sigma = 0.02$ |
| HCN     | Untargeted | 62.0%           | 62.3%           | 50.6%           | 51.4%           |
|         | Targeted   | 79.4%           | 70.8%           | 67.1%           | 58.3%           |
| 2s-AGCN | Untargeted | 51.0%           | 42.2%           | 42.1%           | 40.2%           |
|         | Targeted   | 60.8%           | 50.5%           | 42.2%           | 44.1%           |

Table 4: *Empirical* performance (model accuracy) of our proposed defense on normally trained models.

### 6.3 Additional Experimental Results

*Additional visualization results.* Here we provide more visualization results. We use “drinking water” as the attack target because “drinking water” is a normal action, which looks completely different from the some violent/abnormal actions like throwing, kicking, pushing, and punching. Despite the obvious visual differences between “drinking water” and those abnormal actions, our attack

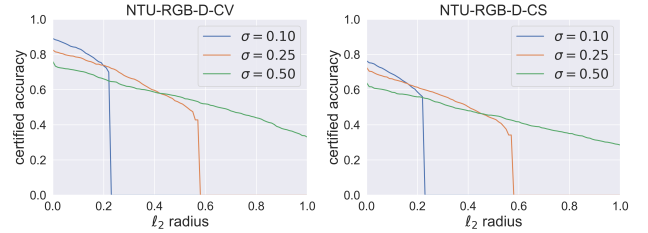


Figure 5: Certification accuracy on HCN

can still fool the state-of-the-art models to recognize those abnormal actions as “drinking water” by imperceptible and reproducible perturbation. In Fig. 6, we show that our attack can fool the HCN model to recognize the “throwing” and “kicking a person” actions as a normal action “drinking water” by imperceptible adversarial perturbation. Similarly, in Fig. 7, we show that our attack can fool the 2s-AGCN model to recognize the “throwing” and “punching a person” actions as a normal action “drinking water”. We also attach the more videos to show the original and adversarial skeleton actions in the supplementary material. These visualization results along with the quantitative results in Table 1 (in the paper) demonstrate that the perturbations are indeed imperceptible and reproducible.

*Kinetics Dataset.* Except for the NTU dataset, we also evaluate our attack on another popular dataset, *i.e.*, Kinetics-400 dataset under both the untargeted and targeted settings. As shown in Table 5, under the untargeted setting, our attack can achieve 100% attack success rates with very small violation of the constraints, similar to its performance on the NTU dataset. However, under the targeted setting, it is much more difficult for our attack to find targeted adversarial skeleton actions with very small violations of the constraints. This is because Kinetics-400 has 400 classes of actions, and the original NTU dataset only has 60 classes of actions. Also, we argue that the results on Kinetics under the targeted setting do not devalue our attack since, even for most of the clean testing samples



| Untargeted | $\beta$ | Kinetics-400 |              |            |              |          |
|------------|---------|--------------|--------------|------------|--------------|----------|
|            |         | Success Rate | $\Delta B/B$ | $\Delta J$ | $\Delta K/K$ | $\ell_2$ |
| HCN        | 0.1     | 100%         | 2.60%        | 0.082      | 1.66%        | 0.150    |
|            | 1.0     | 100%         | 2.58%        | 0.080      | 1.52%        | 0.162    |
|            | 10.0    | 98.8%        | 2.49%        | 0.078      | 1.21%        | 0.145    |
| 2s-AGCN    | 0.1     | 100%         | 0.91%        | 0.053      | 0.58%        | 0.331    |
|            | 1.0     | 100%         | 0.77%        | 0.047      | 0.53%        | 0.298    |
|            | 10.0    | 100%         | 0.75%        | 0.046      | 0.52%        | 0.287    |
| Targeted   | $\beta$ | Kinetics-400 |              |            |              |          |
|            |         | Success Rate | $\Delta B/B$ | $\Delta J$ | $\Delta K/K$ | $\ell_2$ |
| HCN        | 0.1     | 90.2%        | 5.22%        | 0.220      | 11.2%        | 1.864    |
|            | 1.0     | 67.2%        | 2.79%        | 0.124      | 4.86%        | 1.350    |
|            | 10.0    | 17.2%        | 1.44%        | 0.073      | 2.36%        | 0.763    |
| 2s-AGCN    | 0.1     | 99.2%        | 5.25%        | 0.167      | 1.20%        | 0.725    |
|            | 1.0     | 98.8%        | 5.04%        | 0.159      | 1.21%        | 0.722    |
|            | 10.0    | 98.4%        | 4.89%        | 0.153      | 1.03%        | 0.677    |

**Table 5: The performance of our proposed attack on Kinetics: success rate, averaged bone-length difference between original and adversarial skeletons ( $\Delta L/L$ ), averaged joint angle difference (upper bound) ( $\Delta J/J$ ), kinetic energy difference ( $\Delta K/K$ ),  $\ell_2$  distance ( $\ell_2$ ).**

from Kinetics, it is difficult for the state-of-the-models to predict their ground-truth labels (targets).

## 7 CONCLUSION

We study the problem of adversarial vulnerability of skeleton-based action recognition. We first identify and formulate three main constraints that should be considered in adversarial skeleton actions. Since the corresponding constrained optimization problem is intractable, we propose to optimize its dual problem by ADMM, which is a generic method proposed in this paper to generate adversarial examples with complicated constraints. To defend against adversarial skeleton actions, we further specify an efficient defensive inference algorithm and a certification algorithm. The effectiveness of the attack and defense is demonstrated on two opensource models, and the results induce several interesting observations that can help us understand the properties of adversarial skeleton actions.

## REFERENCES

- [1] Maksym Andriushchenko, Francesco Croce, Nicolas Flammarion, and Matthias Hein. 2019. Square Attack: a query-efficient black-box adversarial attack via random search. *arXiv preprint arXiv:1912.00049* (2019).
- [2] Anish Athalye, Nicholas Carlini, and David Wagner. 2018. Obfuscated gradients give a false sense of security: Circumventing defenses to adversarial examples. *arXiv preprint arXiv:1802.00420* (2018).
- [3] José M Bioucas-Dias and Mário AT Figueiredo. 2010. Alternating direction algorithms for constrained sparse regression: Application to hyperspectral unmixing. In *2010 2nd Workshop on Hyperspectral Image and Signal Processing: Evolution in Remote Sensing*. IEEE, 1–4.
- [4] Stéphane Boucheron, Gábor Lugosi, and Pascal Massart. 2013. *Concentration inequalities: A nonasymptotic theory of independence*. Oxford university press.
- [5] Nicholas Carlini and David Wagner. 2017. Towards evaluating the robustness of neural networks. In *Security and Privacy (SP), 2017 IEEE Symposium on*. IEEE, 39–57.
- [6] Guangchun Cheng, Yiwen Wan, Abdullah N Saudagar, Kamesh Namuduri, and Bill P Buckles. 2015. Advances in human action recognition: A survey. *arXiv preprint arXiv:1501.05964* (2015).
- [7] Jeremy M Cohen, Elan Rosenfeld, and J Zico Kolter. 2019. Certified adversarial robustness via randomized smoothing. *arXiv preprint arXiv:1902.02918* (2019).
- [8] Krishnamurthy Dvijotham, Robert Stanforth, Sven Gowal, Timothy A Mann, and Pushmeet Kohli. 2018. A Dual Approach to Scalable Verification of Deep Networks. In *UAI*. 550–559.
- [9] Pedro A Forero, Alfonso Cano, and Georgios B Giannakis. 2010. Consensus-based distributed support vector machines. *Journal of Machine Learning Research* 11, May (2010), 1663–1707.
- [10] Xiang Gao, Wei Hu, Jiaxiang Tang, Jiaying Liu, and Zongming Guo. 2019. Optimized skeleton-based action recognition via sparsified graph regression. In *Proceedings of the 27th ACM International Conference on Multimedia*. 601–610.
- [11] Ian J Goodfellow, Jonathon Shlens, and Christian Szegedy. 2014. Explaining and harnessing adversarial examples. *arXiv preprint arXiv:1412.6572* (2014).
- [12] Leo A Goodman. 1965. On simultaneous confidence intervals for multinomial proportions. *Technometrics* 7, 2 (1965), 247–254.
- [13] Sven Gowal, Krishnamurthy Dvijotham, Robert Stanforth, Rudy Bunel, Chongli Qin, Jonathon Uesato, Timothy Mann, and Pushmeet Kohli. 2018. On the effectiveness of interval bound propagation for training verifiably robust models. *arXiv preprint arXiv:1810.12715* (2018).
- [14] Warren He, James Wei, Xinyun Chen, Nicholas Carlini, and Dawn Song. 2017. Adversarial example defense: Ensembles of weak defenses are not strong. In *11th USENIX Workshop on Offensive Technologies (WOOT 17)*.
- [15] Jinyuan Jia, Xiaoyu Cao, Binghui Wang, and Neil Zhenqiang Gong. 2019. Certified Robustness for Top-k Predictions against Adversarial Perturbations via Randomized Smoothing. *arXiv preprint arXiv:1912.09899* (2019).
- [16] Qijuhong Ke, Mohammed Bannamoun, Senjian An, Ferdous Sohel, and Farid Bousaid. 2017. A new representation of skeleton sequences for 3d action recognition. In *Proceedings of the IEEE conference on computer vision and pattern recognition*. 3288–3297.
- [17] Alexey Kurakin, Ian Goodfellow, and Samy Bengio. 2016. Adversarial machine learning at scale. *arXiv preprint arXiv:1611.01236* (2016).
- [18] Rongjie Lai and Stanley Osher. 2014. A splitting method for orthogonality constrained problems. *Journal of Scientific Computing* 58, 2 (2014), 431–449.
- [19] Mathias Lecuyer, Vaggelis Atlidakis, Roxana Geambasu, Daniel Hsu, and Suman Jana. 2018. Certified robustness to adversarial examples with differential privacy. *arXiv preprint arXiv:1802.03471* (2018).
- [20] Bai Li, Changyou Chen, Wenlin Wang, and Lawrence Carin. 2018. Second-order adversarial attack and certifiable robustness. *arXiv preprint arXiv:1809.03113* (2018).
- [21] Chao Li, Qiaoyong Zhong, Di Xie, and Shiliang Pu. 2018. Co-occurrence feature learning from skeleton data for action recognition and detection with hierarchical aggregation. In *Proceedings of the 27th International Joint Conference on Artificial Intelligence*. 786–792.
- [22] Shuai Li, Wanqing Li, Chris Cook, Ce Zhu, and Yanbo Gao. 2018. Independently Recurrent Neural Network (IndRNN): Building a Longer and Deeper RNN. In *The IEEE Conference on Computer Vision and Pattern Recognition (CVPR)*.
- [23] Jian Liu, Naveed Akhtar, and Ajmal Mian. 2019. Adversarial attack on skeleton-based human action recognition. *arXiv preprint arXiv:1909.06500* (2019).
- [24] Ziyu Liu, Hongwen Zhang, Zhenghao Chen, Zhiyong Wang, and Wanli Ouyang. 2020. Disentangling and unifying graph convolutions for skeleton-based action recognition. *arXiv preprint arXiv:2003.14111* (2020).
- [25] Aleksander Madry, Aleksandar Makelov, Ludwig Schmidt, Dimitris Tsipras, and Adrian Vladu. 2017. Towards deep learning models resistant to adversarial attacks. *arXiv preprint arXiv:1706.06083* (2017).
- [26] Ondrej Miksik, Vibhav Vineet, Patrick Pérez, Philip HS Torr, and F Cesson Sévigné. 2014. Distributed non-convex admm-inference in large-scale random fields. In *British Machine Vision Conference (BMVC)*, Vol. 2.
- [27] Matthew Mirman, Timon Gehr, and Martin Vechev. 2018. Differentiable abstract interpretation for provably robust neural networks. In *International Conference on Machine Learning*. 3575–3583.
- [28] Aditi Raghunathan, Jacob Steinhardt, and Percy Liang. 2018. Certified defenses against adversarial examples. *arXiv preprint arXiv:1801.09344* (2018).
- [29] Amir Shahroudy, Jun Liu, Tian-Tsong Ng, and Gang Wang. 2016. NTU RGB+D: A large scale dataset for 3D human activity analysis. In *Proceedings of the IEEE conference on computer vision and pattern recognition*. 1010–1019.
- [30] Lei Shi, Yifan Zhang, Jian Cheng, and Hanqing Lu. 2019. Skeleton-based action recognition with directed graph neural networks. In *Proceedings of the IEEE Conference on Computer Vision and Pattern Recognition*. 7912–7921.
- [31] Lei Shi, Yifan Zhang, Jian Cheng, and Hanqing Lu. 2019. Two-stream adaptive graph convolutional networks for skeleton-based action recognition. In *Proceedings of the IEEE Conference on Computer Vision and Pattern Recognition*. 12026–12035.
- [32] Chenyang Si, Wentao Chen, Wei Wang, Liang Wang, and Tieniu Tan. 2019. An attention enhanced graph convolutional lstm network for skeleton-based action recognition. In *Proceedings of the IEEE Conference on Computer Vision and Pattern Recognition*. 1227–1236.
- [33] Yusuke Tashiro, Yang Song, and Stefano Ermon. 2020. Output diversified initialization for adversarial attacks. *arXiv preprint arXiv:2003.06878* (2020).

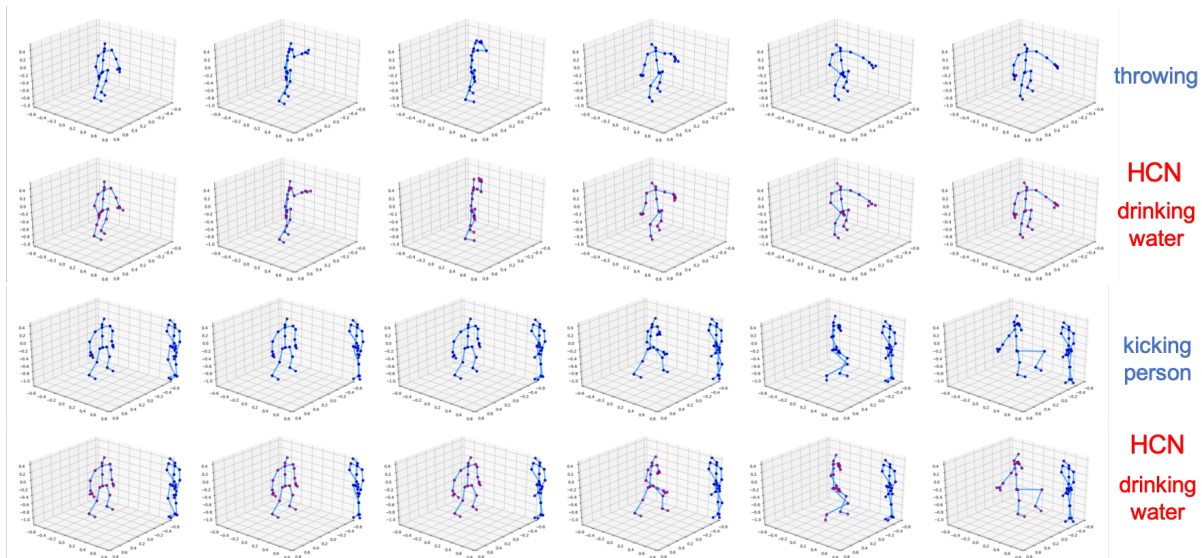


Figure 6: The adversarial skeleton actions generated by our attack under the targeted setting. The generated adversarial skeleton actions are recognized as “drinking water” by the HCN.

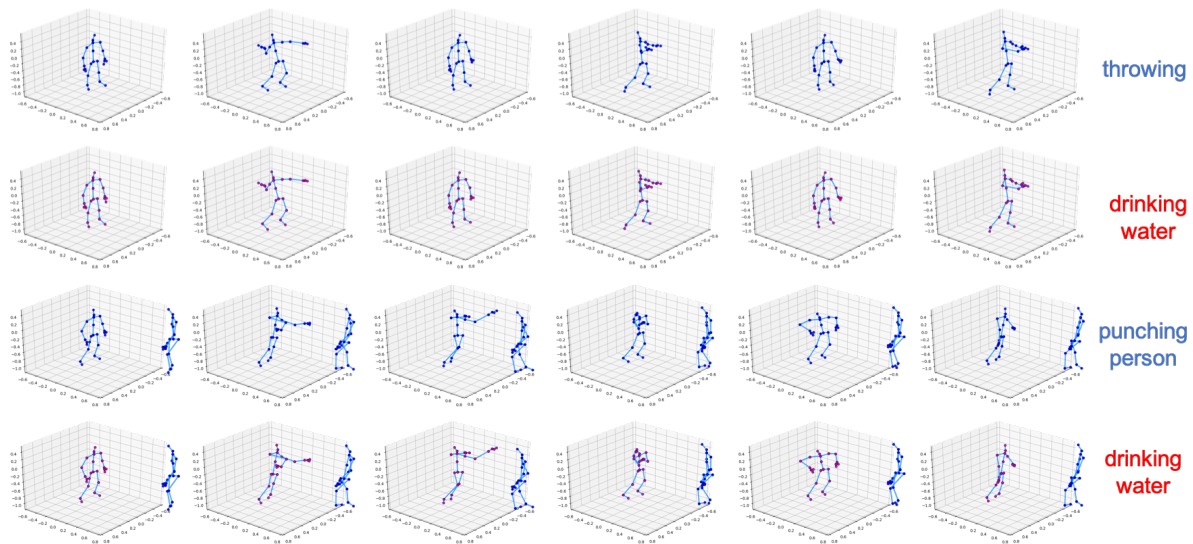


Figure 7: The adversarial skeleton actions generated by our attack under the targeted setting. The generated adversarial skeleton actions are recognized as “drinking water” by the 2s-AGCN.

[34] Jonathan Uesato, Brendan O’Donoghue, Pushmeet Kohli, and Aaron Oord. 2018. Adversarial risk and the dangers of evaluating against weak attacks. In *International Conference on Machine Learning*, 5032–5041.

[35] Pichao Wang, Zhaoyang Li, Yonghong Hou, and Wanqing Li. 2016. Action recognition based on joint trajectory maps using convolutional neural networks. In *Proceedings of the 24th ACM international conference on Multimedia*, 102–106.

[36] Shiqi Wang, Kexin Pei, Justin Whitehouse, Junfeng Yang, and Suman Jana. 2018. Efficient formal safety analysis of neural networks. In *Advances in Neural Information Processing Systems*, 6367–6377.

[37] Yu Wang, Wotao Yin, and Jinshan Zeng. 2019. Global convergence of ADMM in nonconvex nonsmooth optimization. *Journal of Scientific Computing* 78, 1 (2019), 29–63.

[38] Eric Wong and Zico Kolter. 2018. Provable defenses against adversarial examples via the convex outer adversarial polytope. In *International Conference on Machine Learning*, 5283–5292.

[39] Chong Xiang, Charles R Qi, and Bo Li. 2018. Generating 3d adversarial point clouds. *arXiv preprint arXiv:1809.07016* (2018).

[40] Sijie Yan, Yuanjun Xiong, and Dahua Lin. 2018. Spatial temporal graph convolutional networks for skeleton-based action recognition. In *Thirty-Second AAAI Conference on Artificial Intelligence*.

[41] Allen Y Yang, Zihan Zhou, Arvind Ganesh Balasubramanian, S Shankar Sastry, and Yi Ma. 2013. Fast  $\ell_1$ -minimization algorithms for robust face recognition. *IEEE Transactions on Image Processing* 22, 8 (2013), 3234–3246.

[42] Jianyu Yang, Wu Liu, Junsong Yuan, and Tao Mei. 2020. Hierarchical soft quantization for skeleton-based human action recognition. *IEEE Transactions on Multimedia* (2020).

[43] Hongyang Zhang, Yaodong Yu, Jiantao Jiao, Eric P Xing, Laurent El Ghaoui, and Michael I Jordan. 2019. Theoretically principled trade-off between robustness

- and accuracy. *arXiv preprint arXiv:1901.08573* (2019).
- [44] Pu Zhao, Sijia Liu, Yanzhi Wang, and Xue Lin. 2018. An admm-based universal framework for adversarial attacks on deep neural networks. In *Proceedings of the 26th ACM international conference on Multimedia*. 1065–1073.
- [45] Tianhang Zheng, Changyou Chen, and Kui Ren. 2019. Distributionally adversarial attack. In *Proceedings of the AAAI Conference on Artificial Intelligence*, Vol. 33. 2253–2260.